Supplement of Atmos. Chem. Phys., 24, 6339–6357, 2024
https://doi.org/10.5194/acp-24-6339-2024-supplement
© Author(s) 2024. CC BY 4.0 License.

Atmospheric Chemistry and Physics Open Access

Supplement of

Shipborne observations of black carbon aerosols in the western Arctic Ocean during summer and autumn 2016–2020: impact of boreal fires

Yange Deng et al.

Correspondence to: Hiroshi Tanimoto (tanimoto@nies.go.jp)

The copyright of individual parts of the supplement might differ from the article licence.

Text S1: Calculation of ΔO_3 during high BC episodes

Ozone is a major secondary pollutant existing in aged biomass burning plumes (Andreae et al., 1994). The change of ozone concentration from the background level could be a good indicator of the aging of biomass burning plumes. The O_3 concentration in fresh plumes could be lower than that in background. And elevated O_3 from background levels could occur in aged biomass burning plumes. However, this simple approach can be complicated by surface deposition of O_3 during long-range transport (Chin et al., 1994) or less active photochemistry in the fire plumes due to cloudy or rainy weather at the northern high latitude (Tanimoto et al., 2000).

According to GEOS-Chem model simulation, biomass burning dominated all high BC episodes except Episode 9. Therefore, for the high BC episodes identified in the 2017 and 2018 cruises, when O_3 mixing ratios were observed, ΔO_3 was derived to illustrate the aging status of the observed biomass burning airmasses. Here, ΔO_3 was the difference between the observed 1-h O_3 mixing ratios to the Arctic Ocean background, which was calculated as the average 1-h O_3 mixing ratios during the defined BC background periods in 2017 and 2018 cruises (Sect. 4.2) and was estimated to be 25.7 ppb (Fig. S18). The mean and standard deviation of ΔO_3 during E4 to E9 are presented in Table S1. Except Episodes 5 and 9, ΔO_3 during other episodes were on average negative. For E6 and E7, which occurred near the coast of Alaska and back trajectories (Fig. S19) indicate fresh Alaska airmasses could have been captured, it's possible that the monitored biomass burning plumes were fresh that the O_3 production potential have not yet realized. However, lower photochemical activity cannot be excluded as a reason for the lower observed O_3 levels. Back trajectories for E6 (Fig. S19) and E8 (Fig. S11) indicate that the observed airmasses probably have transported more than two days before being monitored. Therefore, O_3 production probably have occurred before the biomass burning plumes were transported to the ship positions if not cloudy or rainy weather and surface deposition may be the main reason for the negative ΔO_3. For Episodes 5 and 9, although the positive ΔO_3 may indicate aged biomass burning plumes were observed, other factors may have dominated the ΔO_3, especially for E9, anthropogenic sources possibly contributed more than biomass burning sources to the observed BC and O_3 as well (Table 3).

Table S1 The mean and standard deviation of ΔO_3 (ppb) during the high BC episodes in 2017 and 2018.

Episodes	E4	E5	E6	E7	E8	E9
Mean	-3.4	2.3	-8.7	-6.5	-4.6	2.0
Standard deviation	2.2	1.5	2.3	4.2	4.8	4.9

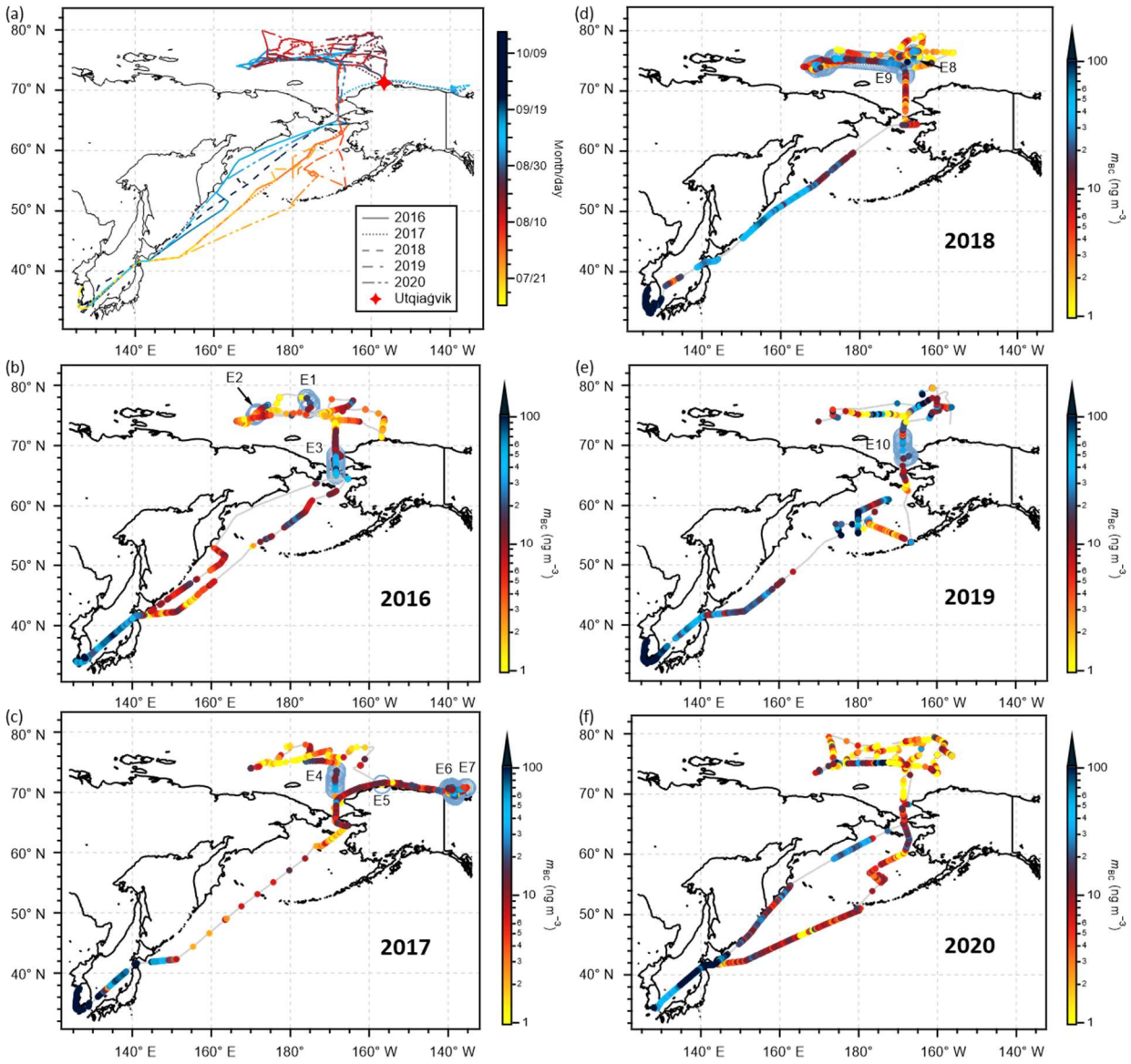

Figure S1 Same as Fig. 1, but for the temporal and spatial distribution of BC mass concentrations along the whole cruise tracks in respective years.

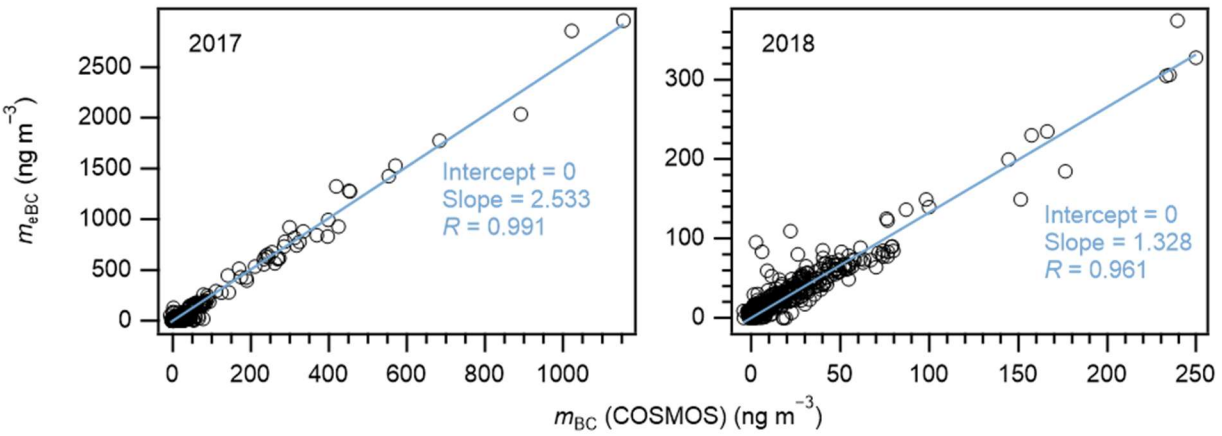

Figure S2 Scatter plot of m_{eBC} versus m_{BC} (COSMOS) for the cruises in 2017 (left) and 2018 (right). In each panel, a linear regression line forced through zero is included. The intercept, slope, and Pearson correlation coefficient (R) are also presented. All data are at a 1-h time resolution.

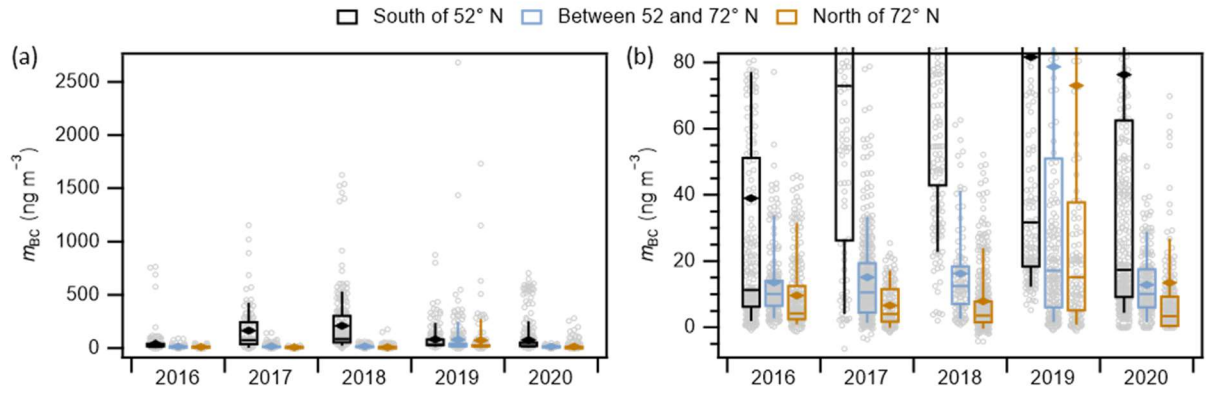

Figure S3 The full-scale view (a) and a zoomed-in view (b) of Fig. 2a.

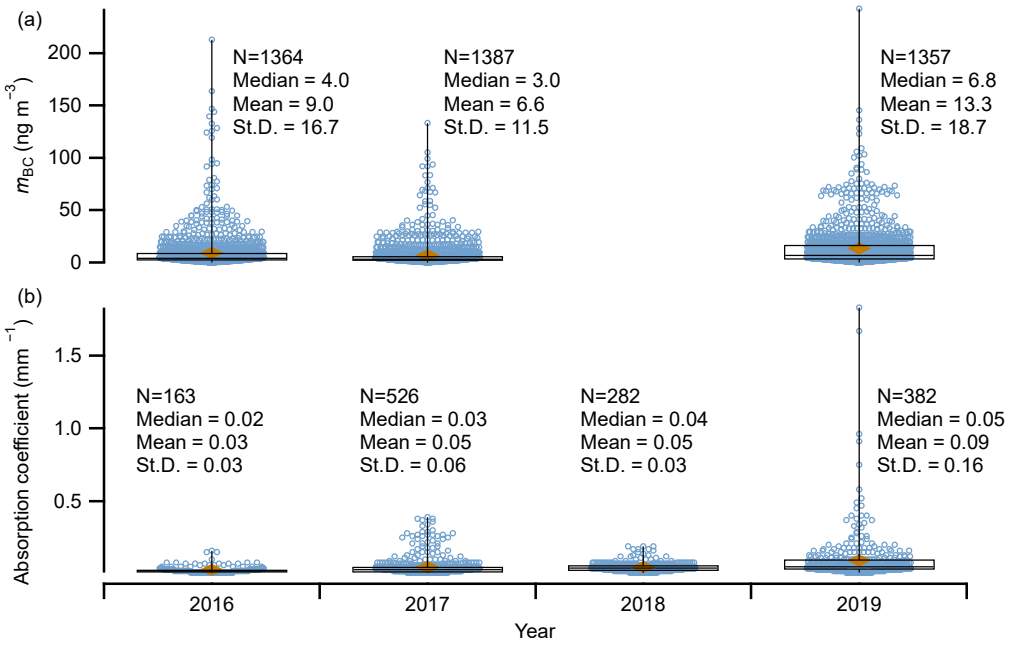

Figure S4 Interannual variations of (a) BC mass concentrations measured by a COSMOS and (b) aerosol absorption coefficients measured by filter-based absorption photometers at Utqiaġvik observatory in August and September. For each box plot, lower whisker – minimum, upper whisker – maximum, box bottom – first quartile, box top – third quartile, line in the box – median, solid diamond marker – arithmetic mean, and circle markers – measured data; N, Median, Mean, and St.D. are the number, median, arithmetic mean, and standard deviation of the data used for the individual box plot, respectively. (Data source: Ohata et al., 2021; https://ads.nipr.ac.jp/dataset/A20201120-001; last access: 8 September 2022.)

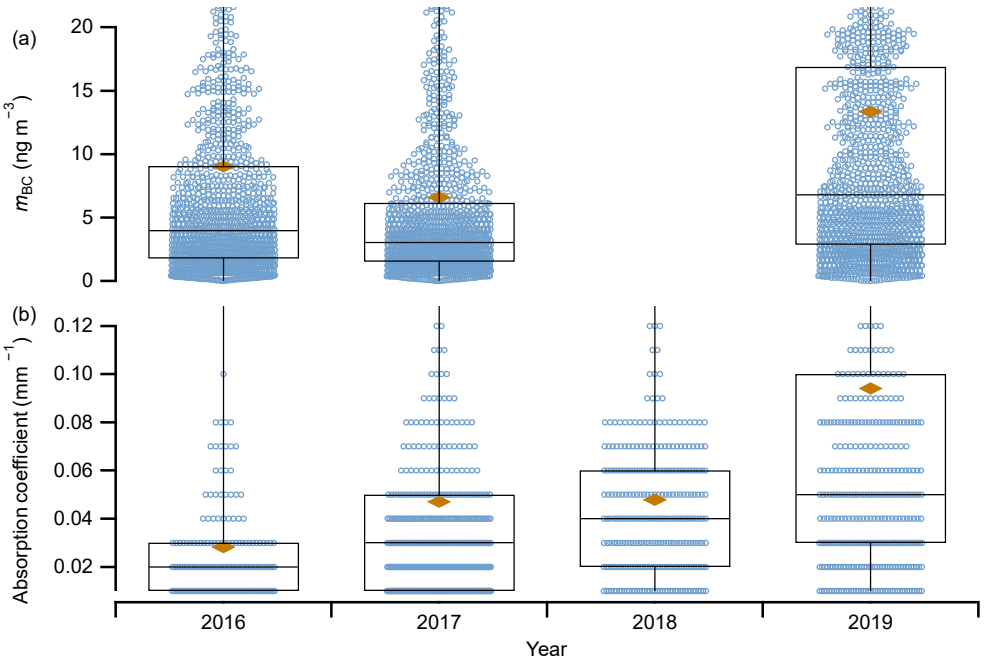

Figure S5 A zoomed-in view of Fig. S4.

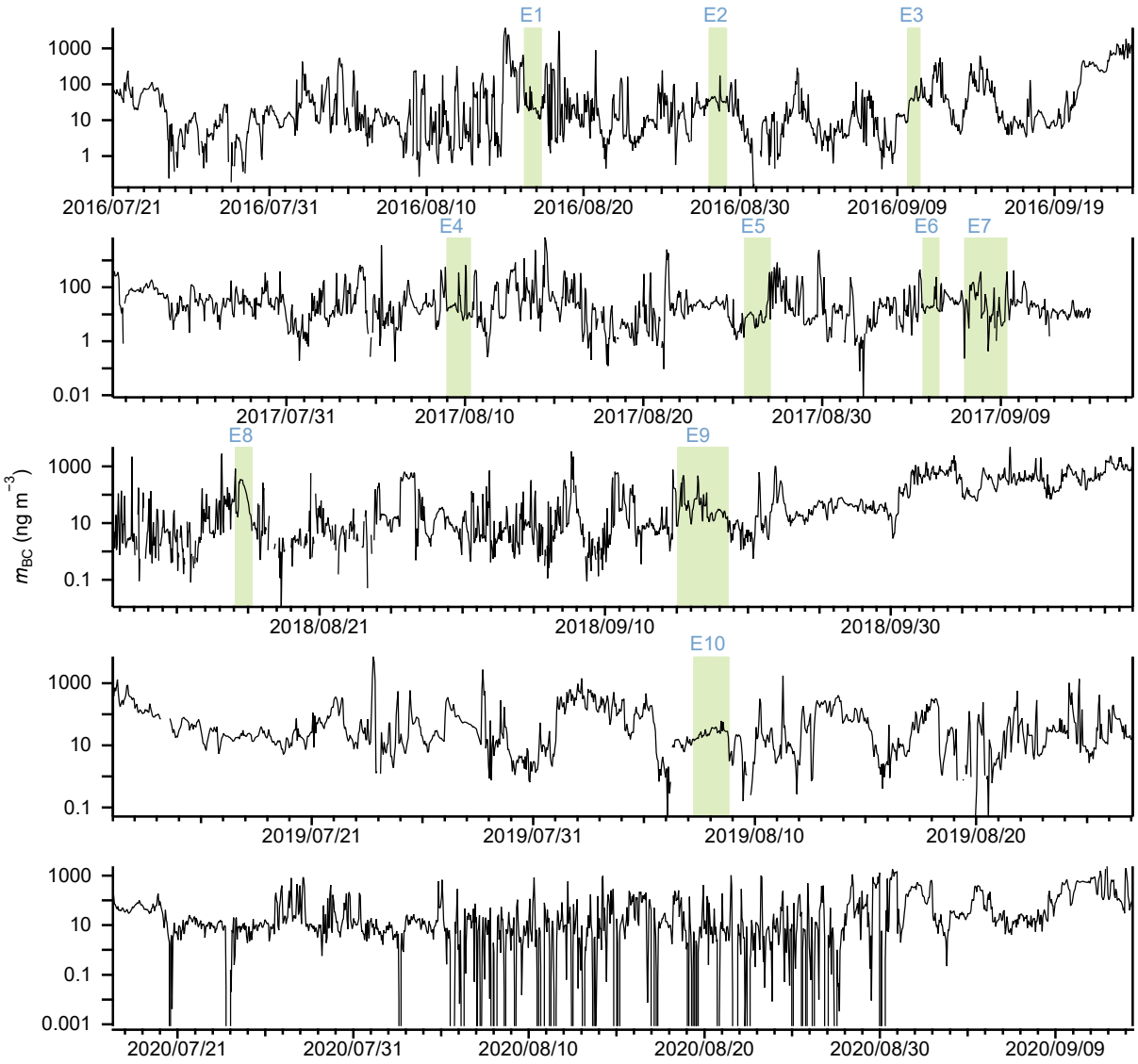

Figure S6 Time series of 1-h BC mass concentrations before removing data influenced by ship exhausts. The shaded areas indicate the 10 episodes selected in this study.

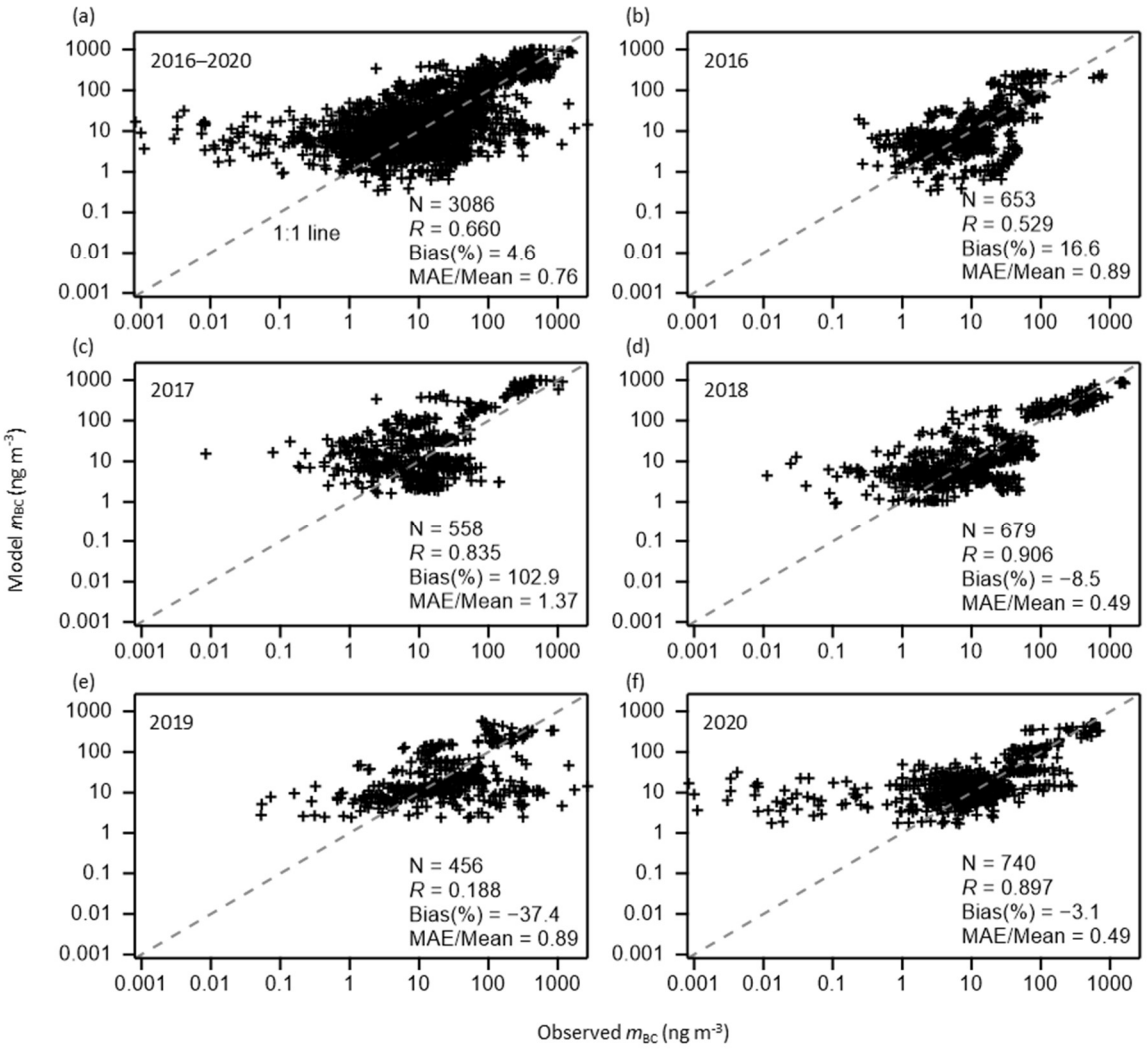

Figure S7 Comparison between model simulated and observed BC mass concentration for all cruises (a) and individual cruises (b-f). Also presented in each panel are the 1:1 line, the number of samples (N), the Pearson correlation coefficient (*R*), the normalized mean bias (%) between the model and observed data, and the ratio of mean absolute error to the mean of m_{BC} (MAE/Mean) for all cruises (a) and individual cruises (b-f).

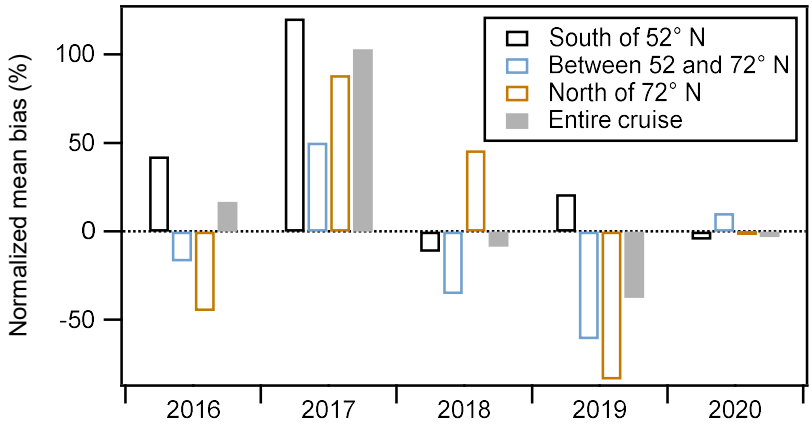

Figure S8 The normalized mean biases (NMB) of the model simulations, based on observed m_{BC} along ship tracks, are presented for latitudes south of 52° N, north of 72° N, and between 52° and 72° N for respective cruises conducted between 2016 and 2020. Additionally, the NMB for the entire duration of each cruise is provided.

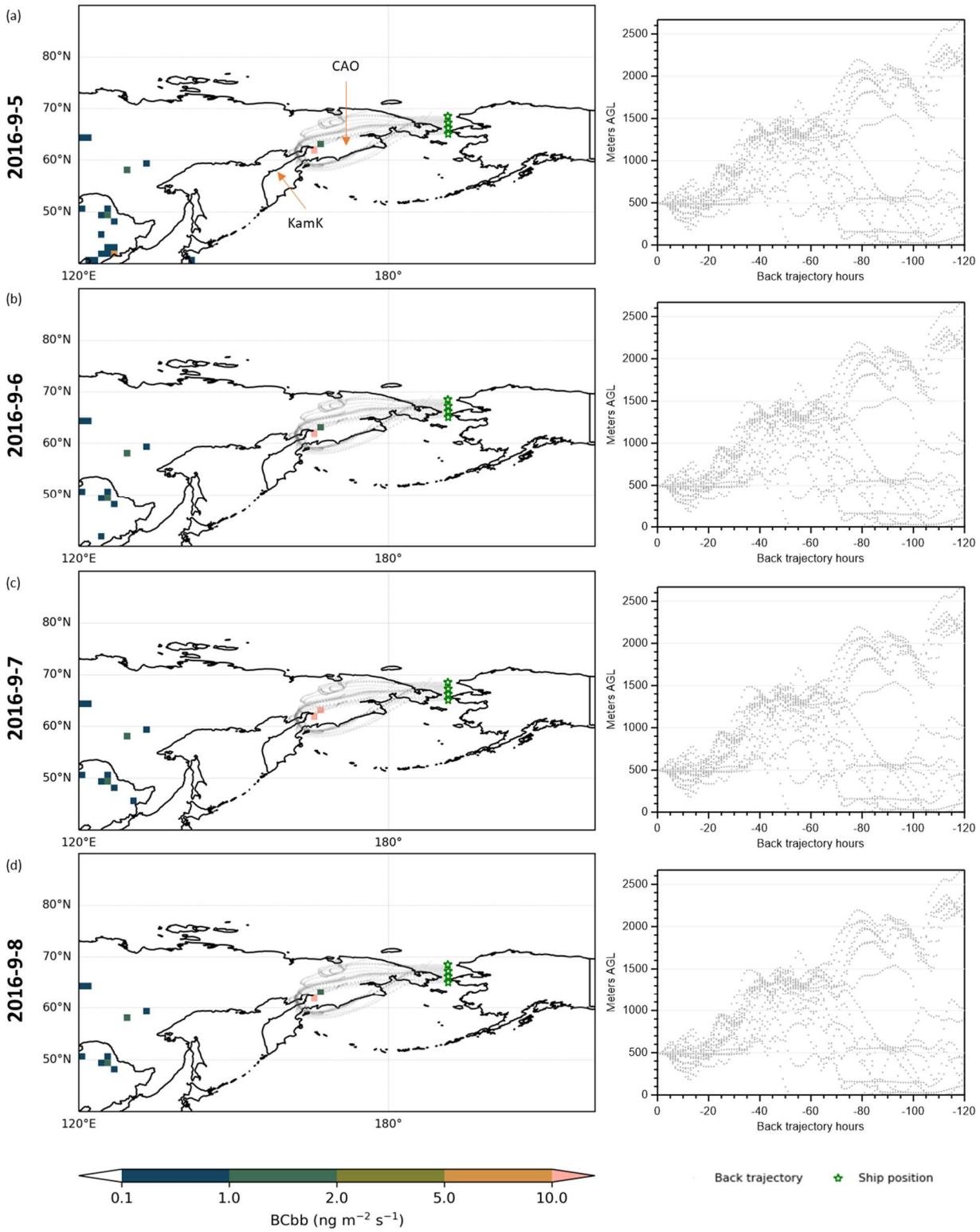

Figure S9 Biomass burning sources of BC (BCbb) during 5–8 September 2016 based on GFED4 data. In each panel, the 5-day airmass back trajectories (dotted lines) started from the ship positions (star markers) during Episode 3 are superimposed on the map, and the height distribution of the back trajectories during

Episode 3 are shown on the right. In panel (a), CAO-Chukotka Autonomous Okrug and KamK-Kamchatka Krai.

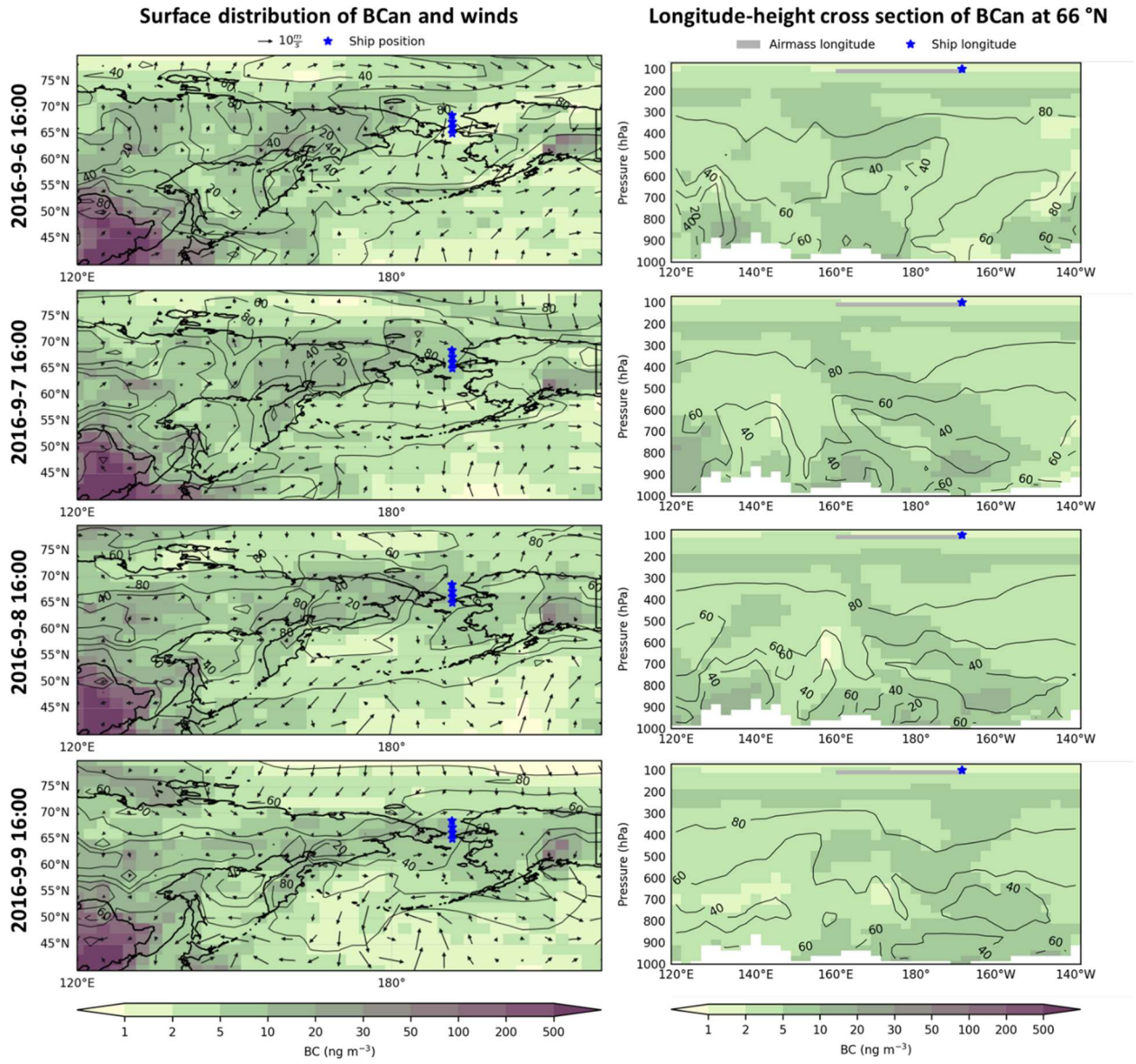

Figure S10 Model simulated anthropogenic BC (BCan, color image) surface distributions (left) and longitude-pressure cross sections at 66° N (right) before Episode 3. Superimposed on the left panels are surface winds and the ship positions. Superimposed on the right panels are the ship longitude positions and the possible transport region of BC-containing air masses related with Episode 3. The latter was inferred from GEOSChem model (Fig. 4) and back trajectories (Fig. S9). On both panels, the contour plot represents the simulated anthropogenic BC to total BC ratio (%).

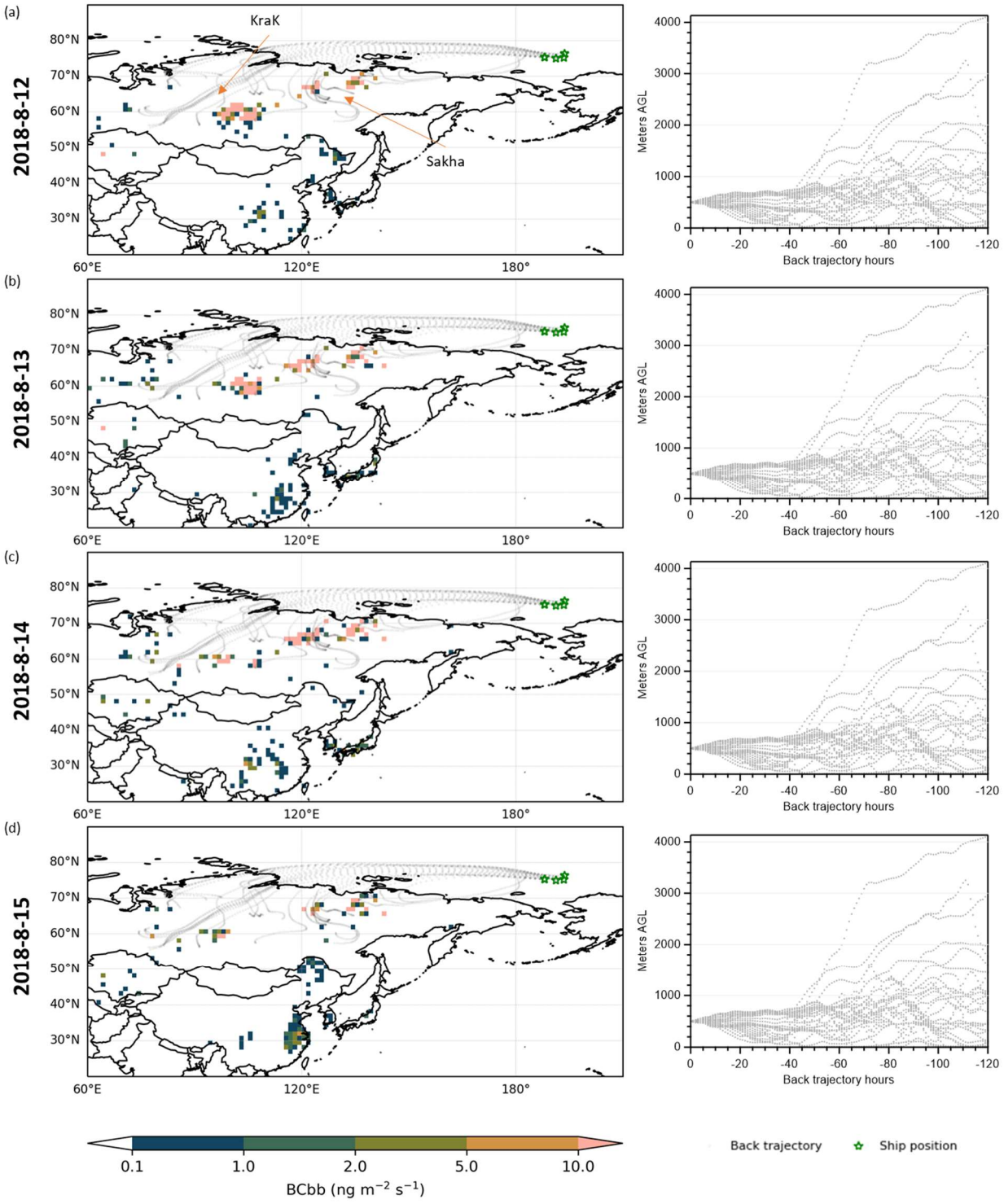

Figure S11 Biomass burning sources of BC (BCbb) during August 12–15, 2018 based on GFED4 data. In each panel, the 5 day airmass back trajectories (dotted lines) started from the ship positions (star markers) during Episode 8 are superimposed on the map, and the height distribution of the back trajectories (dotted lines) during Episode 8 are shown on the right. In panel (a), KraK- Krasnoyarsk Krai and Sakha- the Republic of Sakha.

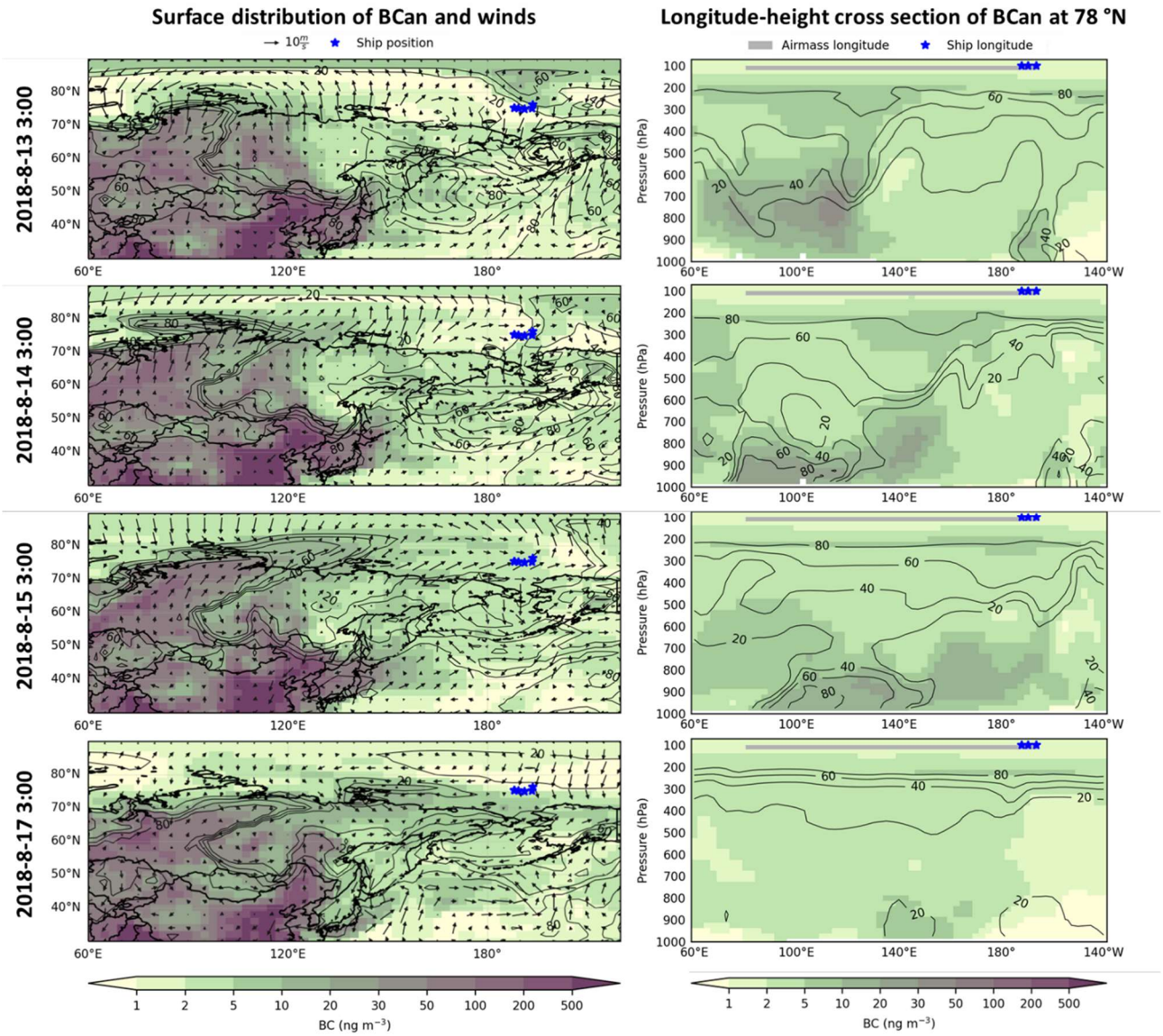

Figure S12 Model simulated anthropogenic BC (BCan, color image) surface distributions (left) and longitude-pressure cross sections at 78° N (right) before to right after Episode 8. Superimposed on the left panels are surface winds and the ship positions. Superimposed on the right panels are the ship longitude positions and the possible transport region of BC-containing air masses related with Episode 8. The latter was inferred from GEOSChem model (Fig. 5) and back trajectories (Fig. S11). On both panels, the contour plot represents the simulated anthropogenic BC to total BC ratio (%).

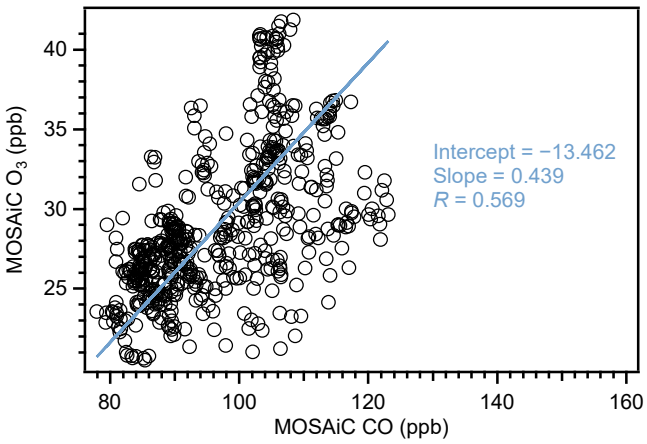

Figure S13 Scatter plot of O_3 versus CO for the period from 6 August 2020 0:00 to 6 September 2020 0:00 of the MOSAiC observation in the central Arctic (Boyer et al., 2023). The line represents the reduced major axis regression: the intercept, slope, and correlation coefficient are also presented. The merged CO and O_3 datasets (Angot et al., 2022) were used for the analysis.

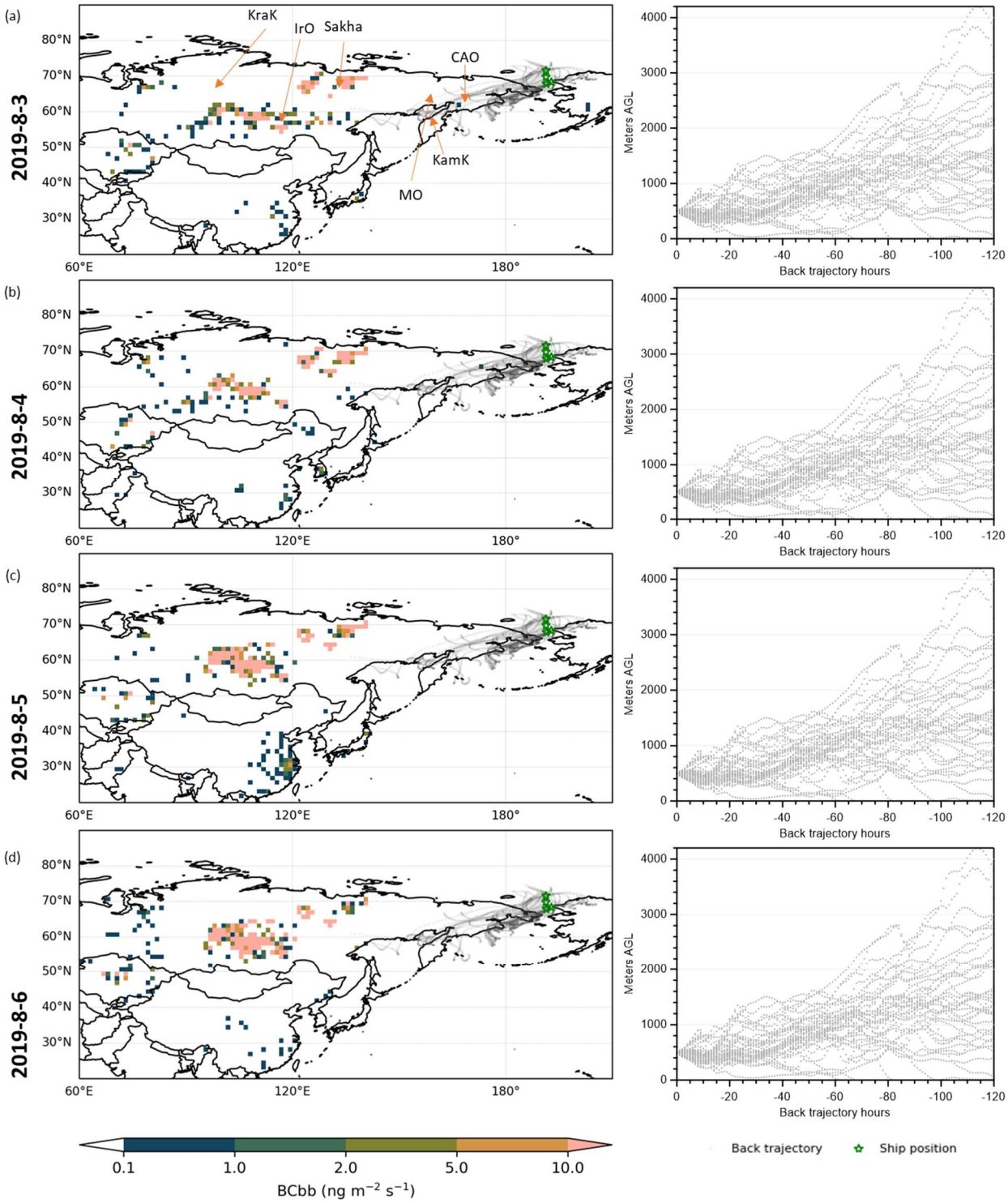

Figure S14 Biomass burning sources of BC (BCbb) during August 3–6, 2019 based on GFED4 data. In each panel, the 5 day airmass back trajectories (dotted lines) started from the ship positions (star markers) during Episode 10 are superimposed on the map, and the height distribution of the back trajectories (dotted lines) during Episode 10 are shown on the right. In panel (a), KraK- Krasnoyarsk Krai, IrO-

Irkutsk Oblast, Sakha- the Republic of Sakha, MO- Magadan Oblast, CAO- Chukotka Autonomous Okrug, and KamK- Kamchatka Krai.

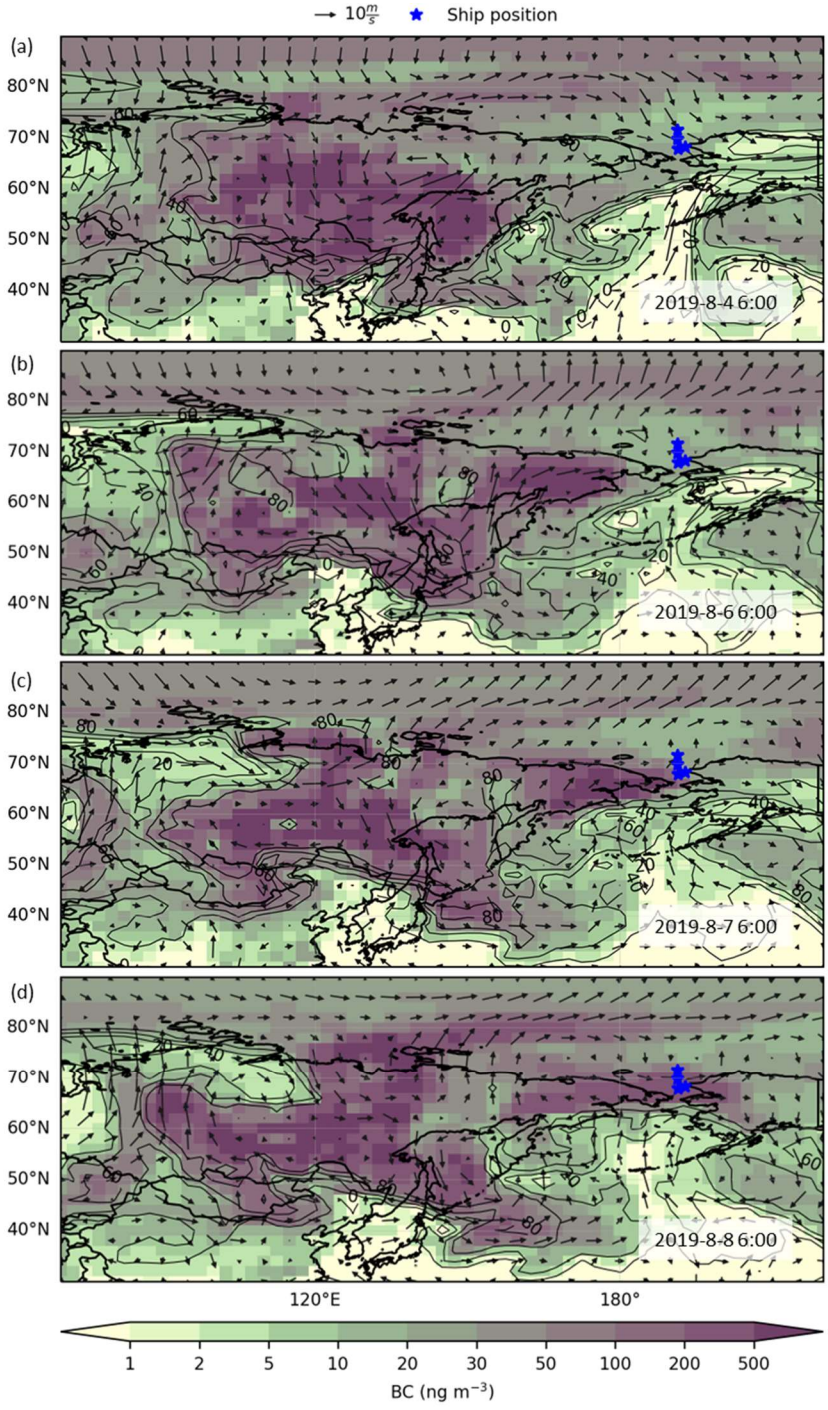

Figure S15 Simulated biomass burning BC (color image) surface distributions and horizontal winds (arrow) at 800 hPa before and during Episode 10. The contour plot superimposed on each panel represents the simulated biomass burning BC to total BC ratio (%). Star markers indicate the ship position during episode 10.

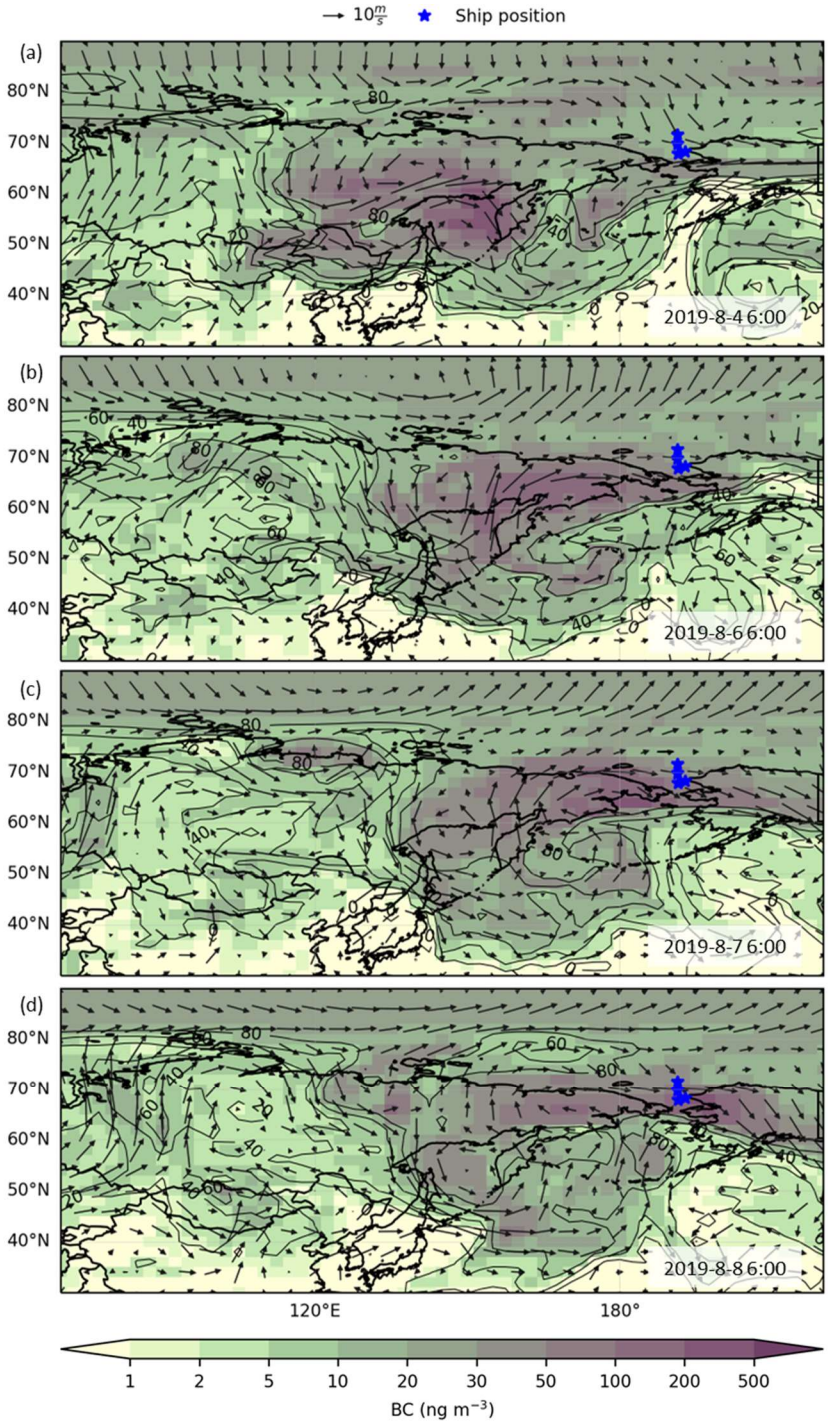

Figure S16 Same as Fig. S15, but for simulations at 600 hPa.

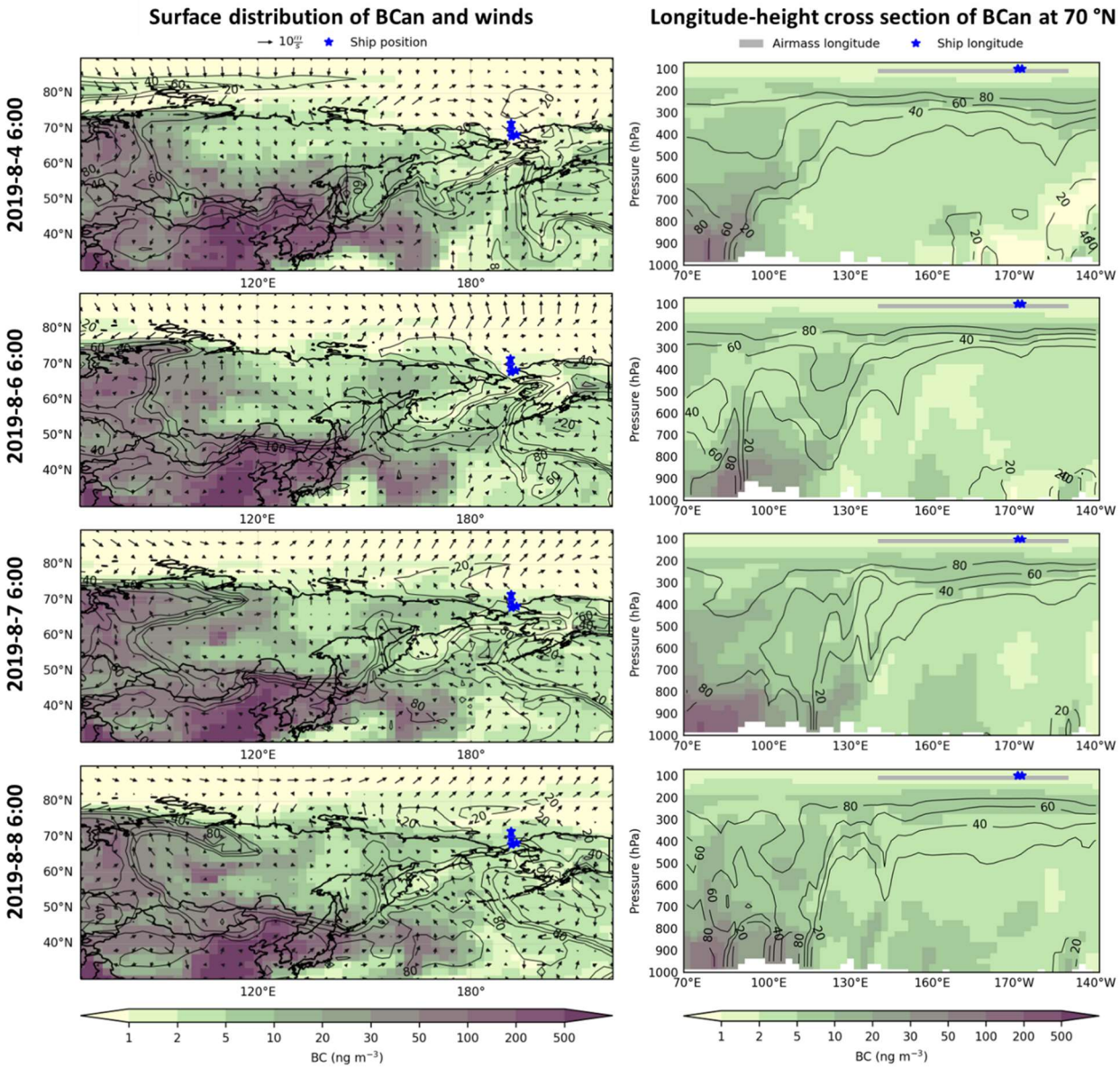

Figure S17 Model simulated anthropogenic BC (BCan, color image) surface distributions (left) and longitude-pressure cross sections at 70° N (right) before and during Episode 10. Superimposed on the left panels are surface winds and the ship positions. Superimposed on the right panels are the ship longitude positions and the possible transport region of BC-containing air masses related with Episode 10. The latter was inferred from GEOSChem model (Fig. 9) and back trajectories (Fig. S14). On both panels, the contour plot represents the simulated anthropogenic BC to total BC ratio (%).

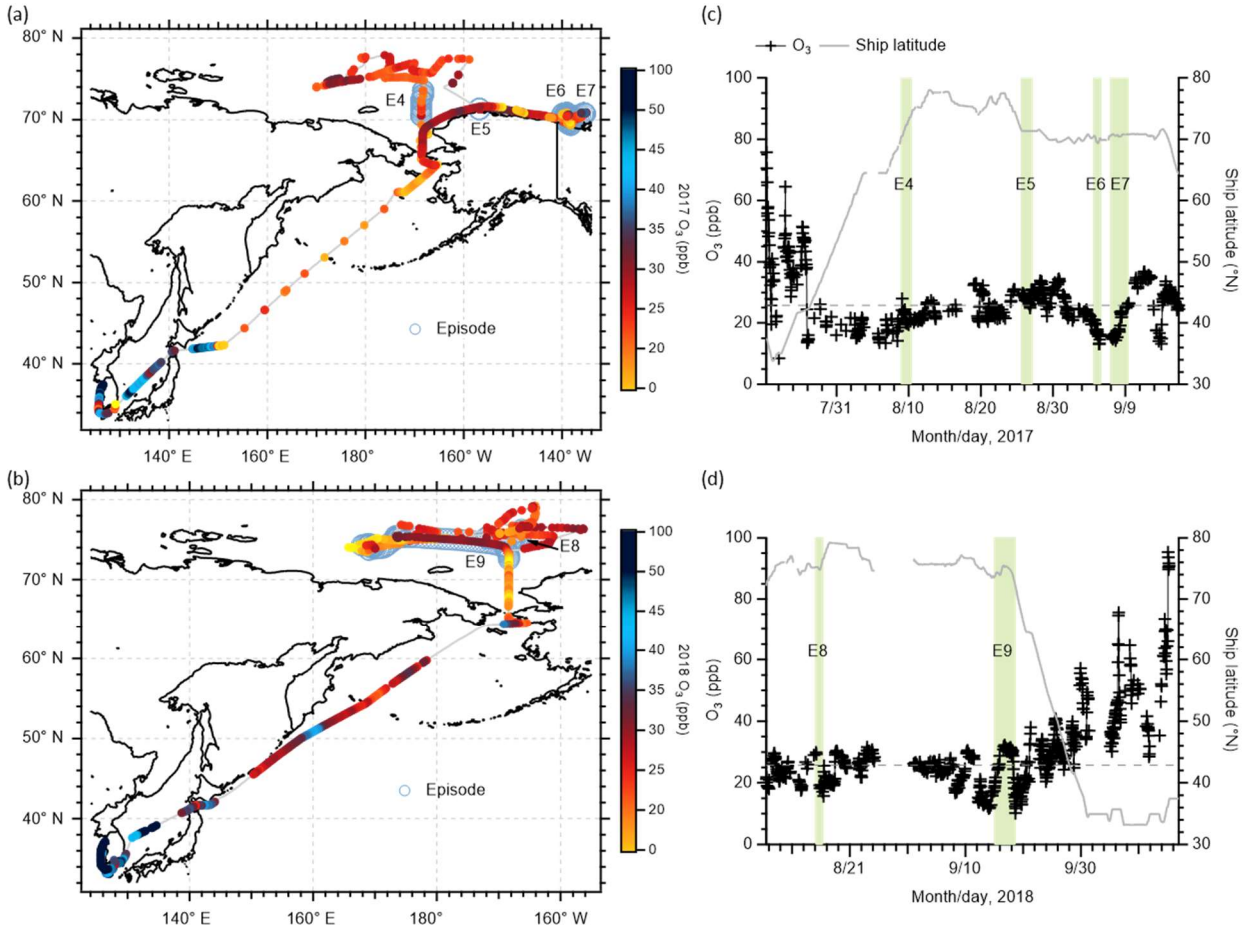

Figure S18 Surface distributions of O_3 mixing ratios along the ship tracks (a and b) and time series of O_3 mixing ratios and ship latitude positions (c and d) during the 2017 (a and c) and 2018 (b and d) cruises. In panels (a) and (b), the grey line represents the cruise track, and the filled color circles superimposed on the track indicate the O_3 mixing ratios. Ship positions during Episodes 4-9 are marked along the ship tracks as open circles. In panels (c) and (d), bar shades indicate Episodes 4-9, and the horizontal dashed lines indicate the background O_3 mixing ratio in the Arctic Ocean (Text S1). The O_3 mixing ratios presented here are at 1 h time resolution and the data influenced by ship exhaust has been removed.

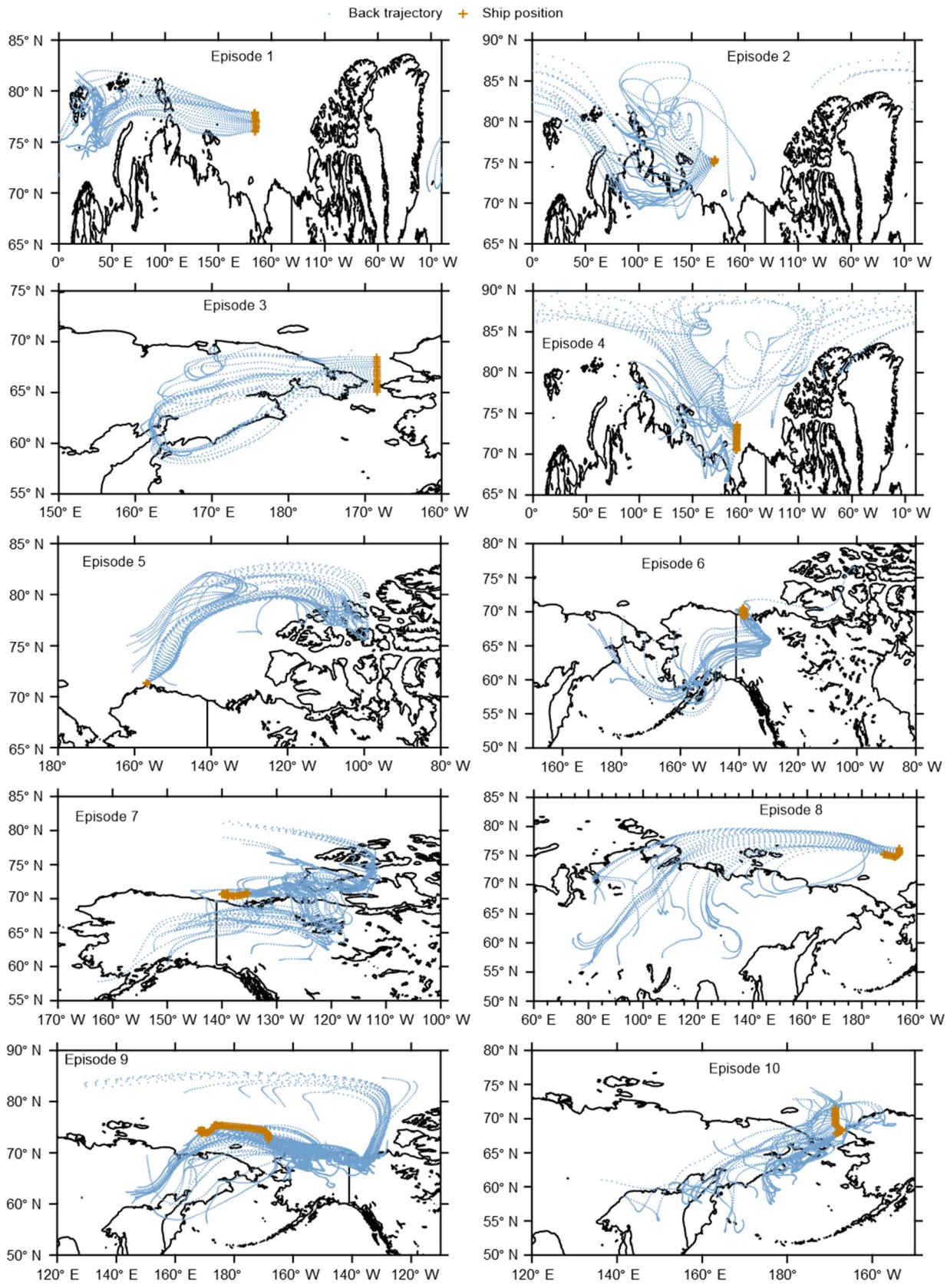
Back trajectory
Ship position
Episode 1
Episode 2
Episode 3
Episode 4
Episode 5
Episode 6
Episode 7
Episode 8
Episode 9
Episode 10

Figure S19 Hourly 5 day backward airmass trajectories (dotted lines) started from 500 m above the ship positions (plus markers) for the ten episodes.

References:

Andreae, M. O., Anderson, B. E., Blake, D. R., Bradshaw, J. D., Collins, J. E., Gregory, G. L., Sachse, G. W., and Shipham, M. C.: Influence of plumes from biomass burning on atmospheric chemistry over the equatorial and tropical South Atlantic during CITE 3, Journal of Geophysical Research: Atmospheres, 99, 12793–12808, https://doi.org/10.1029/94JD00263, 1994.

Angot, H., Blomquist, B., Howard, D., Archer, S., Bariteau, L., Beck, I., Boyer, M., Crotwell, M., Helmig, D., Hueber, J., Jacobi, H.-W., Jokinen, T., Kulmala, M., Lan, X., Laurila, T., Madronich, M., Neff, D., Petäjä, T., Posman, K., Quéléver, L., Shupe, M. D., Vimont, I., and Schmale, J.: Year-round trace gas measurements in the central Arctic during the MOSAiC expedition, Sci Data, 9, 723, https://doi.org/10.1038/s41597-022-01769-6, 2022.

Chin, M., Jacob, D. J., Munger, J. W., Parrish, D. D., and Doddridge, B. G.: Relationship of ozone and carbon monoxide over North America, Journal of Geophysical Research: Atmospheres, 99, 14565–14573, https://doi.org/10.1029/94JD00907, 1994.

Ohata, Sho, Mori, Tatsuhiro, Kondo, Yutaka, Sharma, Sangeeta, Hyvarinen, Antti, Andrews, Elisabeth, Tunved, Peter, Asmi, Eija, Backman, John, Servomaa, Henri, Veber, Daniel, Eleftheriadis, Konstantinos, Vratolis, Stergios, Krejci, Radovan, Zieger, Paul, Koike, Makoto, Kanaya, Yugo, Yoshida, Atsuhi, Moteki, Nobuhiro, Zhao, Yongjing, Tobo, Yutaka, Matsushita, Junji, and Oshima, Naga: Black carbon mass concentrations and aerosol light absorption coefficients measured at Arctic sites (1.01), https://doi.org/10.17592/001.2020112001, 2021.

Tanimoto, H., Kajii, Y., Hirokawa, J., Akimoto, H., and Minko, N. P.: The atmospheric impact of boreal forest fires in far eastern Siberia on the seasonal variation of carbon monoxide: Observations at Rishiri, A northern remote island in Japan, Geophysical Research Letters, 27, 4073–4076, https://doi.org/10.1029/2000GL011914, 2000.